$Nd_{1+\epsilon}Fe_4B_4$: A composition-modulated compound with incommensurate composite crystal structure

A. Bezinge
Département de Physique de la Matière Condensée and Laboratoire de Cristallographie aux Rayons X, Université de Genève, 24 quai E. Ansermet, 1211 Genève 4, Switzerland

K. Yvon
Laboratoire de Cristallographie aux Rayons X, Université de Genève, 24 quai E. Ansermet, 1211 Genève 4, Switzerland

H. F. Braun and J. Muller
Département de Physique de la Matière Condensée, Université de Genève, 24 quai E. Ansermet, 1211 Genève 4, Switzerland

H. -U. Nissen
Laboratorium für Festkörperphysik, Eidgenössische Technische Hochschule Zürich, 8093 Zürich, Switzerland
(Received 16 December 1986; revised manuscript received 24 February 1987)

$Nd_{1+\epsilon}Fe_4B_4$ crystallizes with the tetragonal $Sm_{1+\epsilon}Fe_4B_4$ structure type. It is characterized by two interpenetrating metal substructures with incommensurate translation periods, c_{Nd} and c_{Fe}. The structure is approximated using a superstructure model of composition $Nd_{19}(Fe_4B_4)_{17}$ with $c \simeq 19c_{Nd} \simeq 17c_{Fe} = 66.2(1)$ Å, and refined from single-crystal x-ray data to a consistency index of $R = 0.12$ (2800 contributing reflections, 139 refined parameters). The results reveal rotational and displacive modulations of the Fe tetrahedra chains, Nd atom strings, and B atom pairs. Their periods can be expressed by $L^{rot} = 2L^{dis} = 1/(1/c_{Nd} - 1/c_{Fe})$. High-resolution electron microscopy reveals 17-Å-spaced Moiré-type fringes, but no commensurately spaced structure segments.

I. INTRODUCTION

A ternary boride of composition $NdFe_4B_4$ was found[1,2] to occur as a minor constituent in high-energy product permanent magnets based on $Nd_2Fe_{14}B$. Whether or not it plays a role for magnetic hardening is a matter of controversy.[3,4] Preliminary diffraction studies[5,6] suggested that it belongs to the relatively new class of so-called "composite crystals"[7] which are characterized by mutually incommensurate interpenetrating substructures. In view of the possibly novel physical properties revealed by such crystals, a detailed structural study became desirable.

The existence of $NdFe_4B_4$ was first reported by Chaban *et al.*[8] The compound was characterized in our laboratories and presented[5,6] as a member of the composition-modulated structural series $R_{1+\epsilon}Fe_4B_4$ (R = Ce, Pr, Nd, Sm, Gd, Tb) with variable R content [0.11 (Pr) $\leq \epsilon \leq$ 0.15 (Tb)]. The structures of this series were described in terms of incommensurate Fe- and R-atom substructures with tetragonal symmetry. The translation periods along c of the R substructures, c_R, were smaller by about 10% than those of the Fe substructures, c_{Fe}. They varied as a function of both sample preparation and atomic size of R, thus suggesting that the sublattice translation ratios $k = c_{Fe}/c_R = 1 + \epsilon$ were a measure for the composition of the $R_{1+\epsilon}Fe_4B_4$ crystals.

Recently, the structure of $Nd_{1+\epsilon}Fe_4B_4$ was reinvestigated from single-crystal x-ray data by Givord, Moreau, and Tenaud[9] who confirmed the overall structural features proposed previously, but claimed that the crystals had orthorhombic symmetry and contained commensurate metal-atom substructures, corresponding to the well-defined composition $Nd_5Fe_{18}B_{18}$. Atomic positions (without error estimates) were stated, but not refined.[10,11] Recently a high-resolution microscopic study revealed a tetragonal B-rich phase of approximate composition $Nd_2Fe_7B_6$ and unknown incommensurate structure.[12]

The purpose of the present work was to investigate the structure of $Nd_{1+\epsilon}Fe_4B_4$ in more detail by performing both x-ray-diffraction and high-resolution electron-microscopy experiments. Special attention was given to characterize the incommensurate metal-atom substructures with respect to their modulations as a function of both temperature and composition, and to detect the possible presence of regular stacking faults or commensurately spaced structure segments.

II. EXPERIMENTAL

Samples of various compositions were synthesized from high-purity elements (Nd, $\geq$ 99.9%; Fe, $\geq$ 99.99%, and B, $\geq$ 99.8%) in an arc furnace under argon atmosphere. Those with nominal composition $Nd_{14}Fe_{44}B_{42}$ were remelted in a levitation furnace and extracted by the Czochralski method. A relatively Fe-rich composition was

chosen because the compound formed peritectically at $T_f = 1760(\pm 10)$ °C, as shown by metallurgical investigations. For the x-ray-diffraction studies, two crystals (nos. 1 and 2) were isolated from such a sample, while a third one (no. 3) was taken from another Nd-rich cast sample of composition $Nd_{35}Fe_{20}B_{45}$.

Preliminary diffraction studies by precession method revealed two parallel sets of strong reflections, $(hkl)_{Fe}$ and $(hkl)_{Nd}$, which originated from the Fe and Nd substructures, respectively. In addition, a series of weak satellite reflections appeared in planes parallel to those of the substructure reflections, observable only in diffractometer data.

Lattice parameters and experimental sublattice translation ratios $k = c_{Fe}/c_{Nd}$ were determined for each crystal by precision measurements of the diffraction angles for 32 reflections of each substructure on an automatic four-circle Philips PW 1100 diffractometer (Mo Kα radiation). Crystal no. 1 was chosen for data collection and structure refinement (x-ray 76 program system[13]), because its shape ($64 \times 64 \times 320$ μm^3), made analytical absorption corrections convenient (program ABSCOR). Data were collected by approximating the lattice by a supercell with lattice periods $a = a_{Fe} = a_{Nd} = 7.123$ Å and $c \simeq 8c_{Fe} \simeq 9c_{Nd} = 31.3$ Å. Integrated intensities were measured for one octant in reciprocal space by θ–2θ scans with scan widths of $1.0° + 0.35° \tan\theta$ in the region $3° \leq \theta \leq 35°$. Thus 3500 reflections were collected, of which 1290 had an intensity $I \geq 3\sigma(I)$ including 540 substructure reflections, with maximum values of $h,k = 11$; $l_{Fe} = l_{Nd} = 5$. Among the satellite reflections, only those of first and second order had significant intensities, and those of third and higher orders were not included in the refinements.

High-temperature x-ray-diffraction experiments were performed on powders between 300 and 1200 K under vacuum in order to detect a possible variation of the sublattice translation ratio $k = c_{Fe}/c_{Nd}$ as a function of temperature. For this purpose reflections up to $2\theta = 70°$ were measured on a Philips flat-sample powder diffractometer using Cu Kα radiation.

For the high-resolution electron microscopy studies, a large crystal (a few cubic millimeters) previously examined by metallography was crushed to 80-μm mesh powder and dispersed on microgrids covered with carbon. A Jeol JEM200 CX transmission electron microscope operating at 200 kV with a $\pm 10°$ top-entry tilting stage was used. All images were made by inserting a 40-μm objective aperture corresponding to an ideal resolution of 0.68 $Å^{-1}$. The spherical-aberration constant was $C_s = 1.2$ mm. The observed images were simulated for different sample thickness and defocus values by means of the multislice method,[14,15] using a computer program adapted for large unit cells.[16]

III. RESULTS

A. x-ray diffraction

A preliminary analysis of the diffraction data confirmed that $Nd_{1+\epsilon}Fe_4B_4$ was isostructural to $Sm_{1+\epsilon}Fe_4B_4$.[6] Lattice parameters and intensity equivalent reflections measured on various crystals indicated tetragonal symmetry. The intensities of the two sets of substructure reflections were consistent with the assumption of two metal substructures containing, respectively, chains of edge-sharing Fe-atom tetrahedra with attached B-atom dumbbells, and strings of Nd atoms. The satellite reflections indicated that both substructures were modulated. The existence of modulations along the tetragonal axis can be seen from the intensity scan represented in Fig. 1.

The refined lattice parameters a, c_{Fe}, and c_{Nd} for the three crystals investigated are summarized in Table I. The sublattice translation ratios $k = c_{Fe}/c_{Nd}$ could not be approximated by ratios of small integer values, m/n.

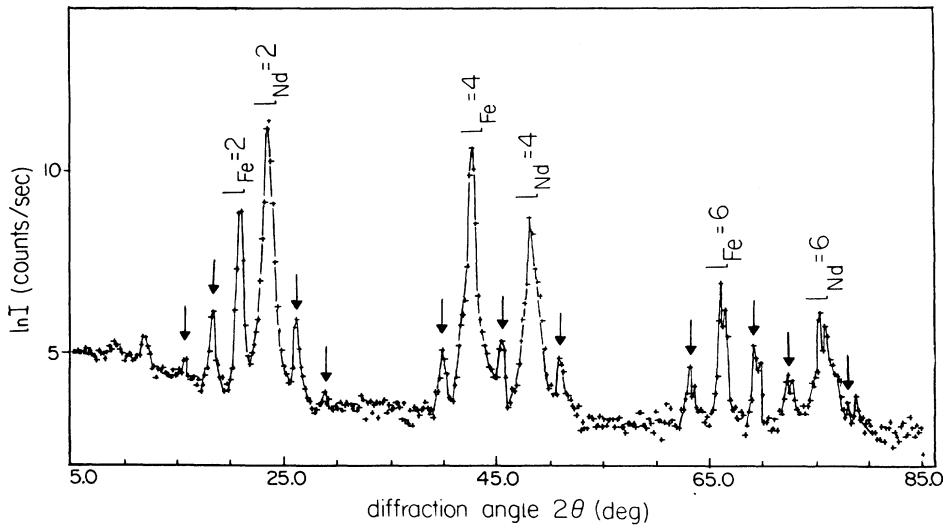

FIG. 1. X-ray-diffraction scan along c* for crystal 1. Fe and Nd substructure reflections are marked l_{Fe} and l_{Nd}, satellites are marked by arrows. Doublets at high angles are due to the separation of the Mo Kα_1 and Mo Kα_2 radiation.

TABLE I. Tetragonal lattice parameters and sublattice translation ratios $k = c_{Fe}/c_{Nd}$ for three $Nd_{1+\epsilon}Fe_4B_4$ crystals. For the calculation of the periods of the rotational modulation, L^{rot}, see text. Estimated standard deviations are given in parentheses.

	Crystal 1	Crystal 2	Crystal 3
a (Å)	7.1226(1)	7.1233(1)	7.1244(1)
c_{Fe} (Å)	3.9025(1)	3.9042(1)	3.9077(1)
c_{Nd} (Å)	3.4792(1)	3.4512(1)	3.4227(1)
c_{Fe}/c_{Nd}	1.1217(1)	1.1313(1)	1.1417(1)
L^{rot} (Å)	32.076(2)	29.744(2)	27.577(2)

TABLE II. Fit between the experimental positions of 00l reflections, and those calculated from a model with superlattice period $c \simeq mc_{Nd} \simeq nc_{Fe}$. Ratios of m and n are chosen to fit the experimental sublattice translation ratio, $m/n \simeq k = c_{Fe}/c_{Nd} = 1.1217(1)$ for crystal 1.

m/n	$(m/n)-k$	Error of fit	c (Å)
$\frac{37}{33}$ (=1.1212)	−0.0005	0.62	128.79(4)
$\frac{9}{8}$ (=1.1250)	+0.0033	1.08	31.27(2)
$\frac{19}{17}$ (=1.1176)	−0.0041	1.73	66.24(5)
$\frac{10}{9}$ (=1.1111)	−0.0106	4.03	34.97(7)

Furthermore the translation periods of the Nd substructure, c_{Nd}, differed significantly from one crystal to the other. On the other hand, measurements as a function of temperature showed no significant variations of k. The k values measured on powders varied from $k = 1.120(2)$ to 1.118(3) between 300 and 1200 K. Those measured at 100 K on single crystals were practically identical to those measured at 300 K.

In view of these results, an incommensurate structure model with four reciprocal lattice vectors, $\mathbf{g} = h\mathbf{a}^* + k\mathbf{b}^* + l_{Fe}\mathbf{c}^*_{Fe} + l_{Nd}\mathbf{c}^*_{Nd}$, was introduced, which allowed us to index both the substructure and the satellite reflections.[7,17] However, due to the absence in our laboratory of a suitable computer program to refine such a model, the structure was approximated with a three-dimensional superstructure model[5,6] of composition $Nd_m(Fe_4B_4)_n$ with a superlattice period $c = nc_{Fe} = mc_{Nd}$ (m,n are the numbers of sublattice translations). The ratio m/n was related to the sublattice translation ratio k and to the observed Nd content $1+\epsilon$ by $m/n \simeq c_{Fe}/c_{Nd} = k = 1+\epsilon$. For the description of this model, space group $P4_2/n$ [No. 86 (Ref. 18)] was chosen, because it is the only common maximal nonisomorphic subgroup of the space groups used to describe the average (i.e., nonmodulated) Fe substructures ($P4_2/ncm$) and Nd substructures ($I4/mmm$).

In order to obtain the most suitable values of m and n for crystal no. 1, diffraction angles calculated from this model were fitted on the positions of the diffraction maxima measured on the scan along $\mathbf{c}^*$ (Fig. 1). The results of different fits are summarized in Table II. The best fit for small integer values was that for $m = 37$ and $n = 33$. A refinement of the corresponding structure model failed, however, presumably because of the large number of atomic positional parameters (348) and their correlations. A structure model with values corresponding to the second best fit ($m = 9$, $n = 8$) could not be constructed in space group $P4_2/n$ as m and n need to be odd. Thus the model yielding the third-best fit, i.e., that for $m = 19$ and $n = 17$, was chosen for structure refinement. By comparison, the fit with $m = 10$ and $n = 9$, i.e., that corresponding to the orthorhombic model,[11] was very poor and precluded such a model from structure refinement.

The refinement (isotropic temperature factors and positional parameters) of the model, with $m = 19$ and $n = 17$, converged to a consistency index of $R = \sum(F_{obs} - F_{calc})/\sum(F_{obs}) = 0.12$ (for 2800 contributing reflections and 139 refined parameters). The consistency indices of the Fe and Nd substructure reflections were $R_{Fe} = 0.05$ and $R_{Nd} = 0.04$. Due to problems with parameter correlations, the z(Nd) values were refined from 00l data only and fixed during the final stage of structure refinement. Atomic parameters are summarized in Table III, and a structural drawing is represented in Fig. 2. A list of interatomic distances and of observed and calculated structure factors can be obtained from the authors. In order to verify the compositional metal-atom ratio [Nd]/[Fe_4], a refinement of the Nd atom sites was made in a projection on the basal plane by using $hk0$ reflections only. The result, [Nd]/[Fe_4] = 1.14(6), was consistent with the results of the microprobe analysis [1.09(1)].[6]

The metal- and boron-atom substructures show both a rotational and a displacive type of modulation. The rotational modulation around $\mathbf{c}$ of the Fe-atom tetrahedra chains and B-atom pairs can be seen in the structural drawing represented in Fig. 2, whereas their displacive modulation along $\mathbf{c}$, as well as that of the Nd-atom strings, can be seen only from a numerical analysis of the atomic coordinates. The rotational modulation of the Fe-atom tetrahedra and B-atom pairs has an amplitude of ±7(1)° [corresponding to maximum atomic dislacements of ±0.16(2) Å]. Its period along $\mathbf{c}$ is $L^{rot} \simeq 33$ Å $= c/2$, thus covering about 8.5 Fe double tetrahedra. The displacive modulation of the Fe atoms has an amplitude of $dz_{Fe} = \pm 0.06(1)$ Å and a period which is half of that of the rotational modulation, $L^{dis}_{Fe} = L^{rot}/2 = 16.5$ Å. The displacive modulation of the Nd-atom strings has a period identical to that of the Fe-atom substructure, $L^{dis}_{Nd} = L^{dis}_{Fe}$, and an amplitude of $dz_{Nd} = \pm 0.05(2)$ Å.

B. High-resolution electron microscopy

A diffraction pattern taken near the crystal edge along [110] and the corresponding structure image are represented in Figs. 3 and 4, respectively. The strong spots in Fig. 3(a), marked $(hkl)_{Fe}$, originate from the Fe substructure. They do not obey the kinematical reflection conditions as observed on the x-ray patterns (00l with $l = 2n$ only), due to the loss of the fourfold screw axis (4_2) projected on the diffraction plane.[19] On both sides of the

Fe substructure spots, satellite reflections appear in directions approximately parallel to [001]. They are generally weak, except those which can be attributed to the Nd substructure, marked $(hkl)_{Nd}$ [see also enlarged portion of pattern in Fig. 3(b)]. In diffraction patterns taken on other crystals, these satellites are exactly parallel to the [001] direction, but the corresponding structure images show poor contrast, presumably because of the larger sample thickness. The reciprocal distances between satellites and Fe substructure spots correspond to multiples of the effective reciprocal lattice vector,[20] $\Delta c^* = 2c^*_{Nd} - 2c^*_{Fe} \simeq \frac{1}{17}$ Å^{-1}. The fact that these satellites are present on both sides of the Fe substructure spots along [001] is characteristic for the presence of a density modulation due to the superposition of the two metal substructures with different translation periods along that direction.[21,22]

The structure image shown in Fig. 4 consists of a regular mesh of white dots, which corresponds to the Fe sub-

TABLE III. Atomic coordinates from the structure refinement of crystal 1 with the supercell $c \simeq 19c_{Nd} \simeq 17c_{Fe} = 66.2(1)$ (Å), estimated standard deviations are given in parentheses. All isotropic temperature factors $\langle u^2 \rangle \leq 1 \times 10^{-2}$ Å^2.

Atom	x	y	z
Nd-1	0.75	0.75	0.0400(—)
Nd-2	0.75	0.75	0.0925(—)
Nd-3	0.75	0.75	0.1444(—)
Nd-4	0.75	0.75	0.1967(—)
Nd-5	0.75	0.75	0.2500(—)
Nd-6	0.75	0.75	0.5134(—)
Nd-7	0.75	0.75	0.5662(—)
Nd-8	0.75	0.75	0.6184(—)
Nd-9	0.75	0.75	0.6708(—)
Nd-10	0.75	0.75	0.7234(—)
Fe-1	0.129(1)	0.632(1)	0.0210(1)
Fe-2	0.136	0.884	0.0505
Fe-3	0.137	0.623	0.0805
Fe-4	0.127	0.872	0.1100
Fe-5	0.133	0.609	0.1401
Fe-6	0.126	0.863	0.1686
Fe-7	0.142	0.604	0.1980
Fe-8	0.120	0.869	0.2271
Fe-9	0.143	0.622	0.2561
Fe-10	0.119	0.872	0.2859
Fe-11	0.137	0.628	0.3153
Fe-12	0.134	0.883	0.3456
Fe-13	0.128	0.626	0.3747
Fe-14	0.143	0.888	0.4042
Fe-15	0.113	0.630	0.4334
Fe-16	0.145	0.878	0.4627
Fe-17	0.108	0.632	0.4916
B-1	0.525(3)	0.423(3)	0.0383(3)
B-2	0.554(3)	0.419(3)	0.0943(4)
B-3	0.618(9)	0.334(9)	0.1489(10)
B-4	0.678(13)	0.553(13)	0.2000(13)
B-5	0.679(18)	0.486(18)	0.2511(19)
B-6	0.594(10)	0.475(10)	0.3296(10)
B-7	0.586(5)	0.417(5)	0.3901(5)
B-8	0.581(15)	0.361(15)	0.4671(16)
B-9	0.558(4)	0.402(4)	0.5087(4)
B-10	0.607(10)	0.314(10)	0.5422(10)
B-11	0.554(3)	0.422(3)	0.6266(3)
B-12	0.580(3)	0.429(3)	0.6846(3)
B-13	0.586(2)	0.452(2)	0.7434(2)
B-14	0.578(4)	0.458(4)	0.8026(4)
B-15	0.578(3)	0.451(3)	0.8603(4)
B-16	0.555(4)	0.420(4)	0.9207(4)
B-17	0.550(3)	0.434(3)	0.9779(4)

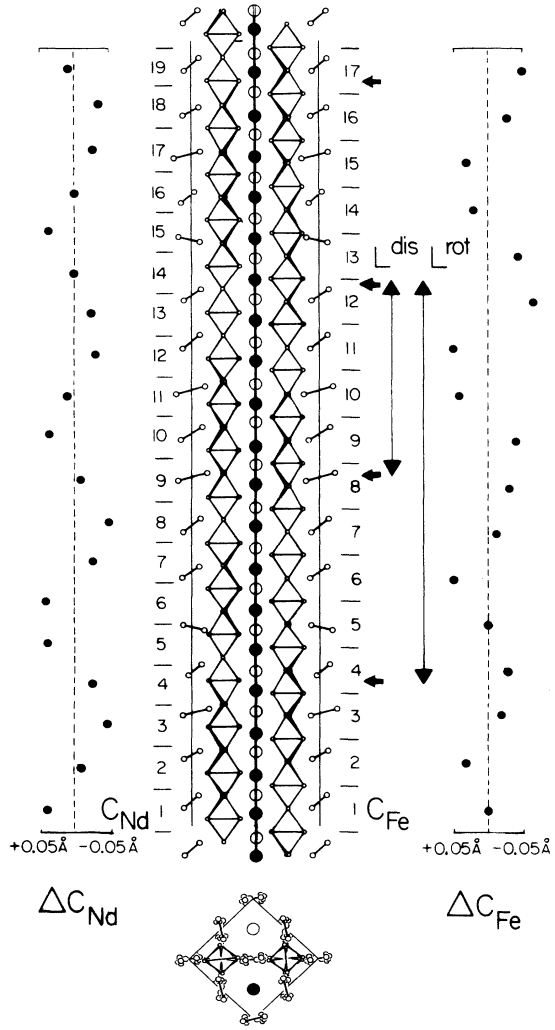

FIG. 2. Structure of $Nd_{1+\epsilon}Fe_4B_4$ as described by the supercell $c \simeq 19c_{Nd} \simeq 17c_{Fe} = 66.2(1)$ Å, viewed along [110]. Large open and solid circles, Nd. Tetrahedra chains, Fe. Dumbbells, B. Note that this drawing differs from those given in Refs. 10 and 11, which have different scales along and perpendicular to the Fe chain axis. The displacement modulations are represented graphically, by plotting the differences (Δc_{Nd}, Δc_{Fe}) between the refined and the average separation values along c.

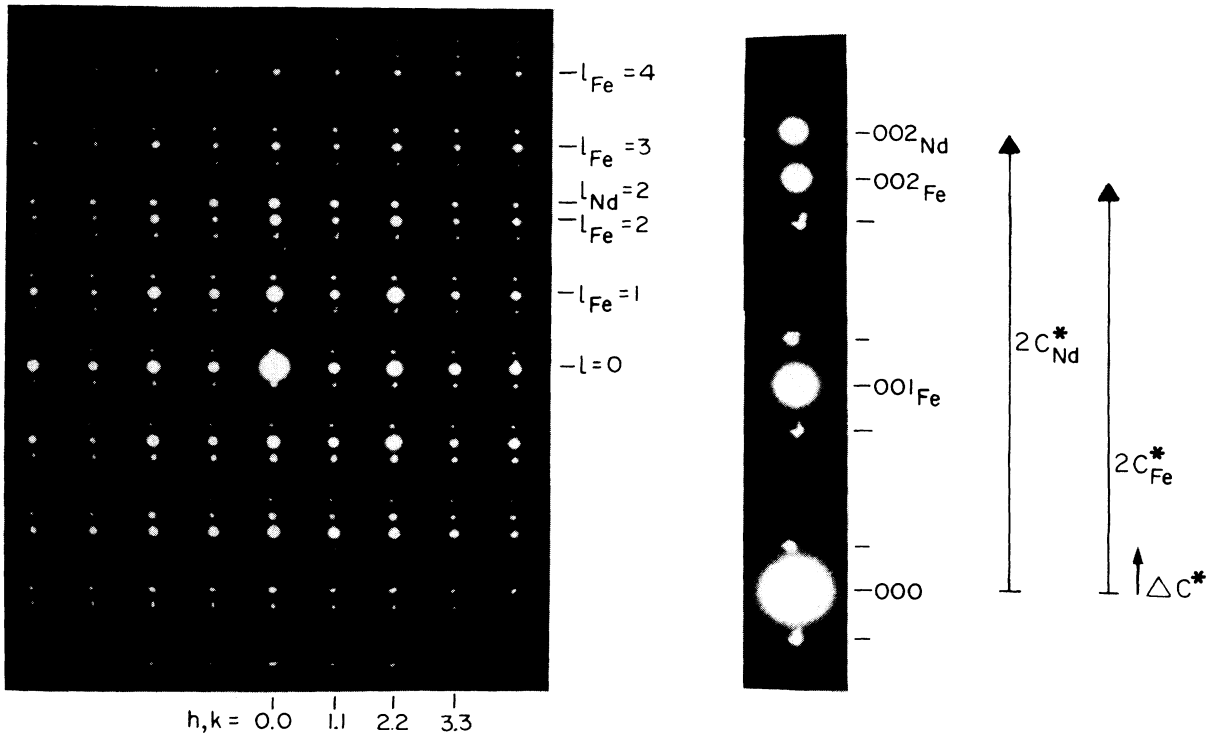

FIG. 3. (a) Electron-microscope diffraction image of $Nd_{1+\epsilon}Fe_4B_4$ along [110], with [001] as the vertical axis. (b) Enlarged portion of the diffraction image shown in (a).

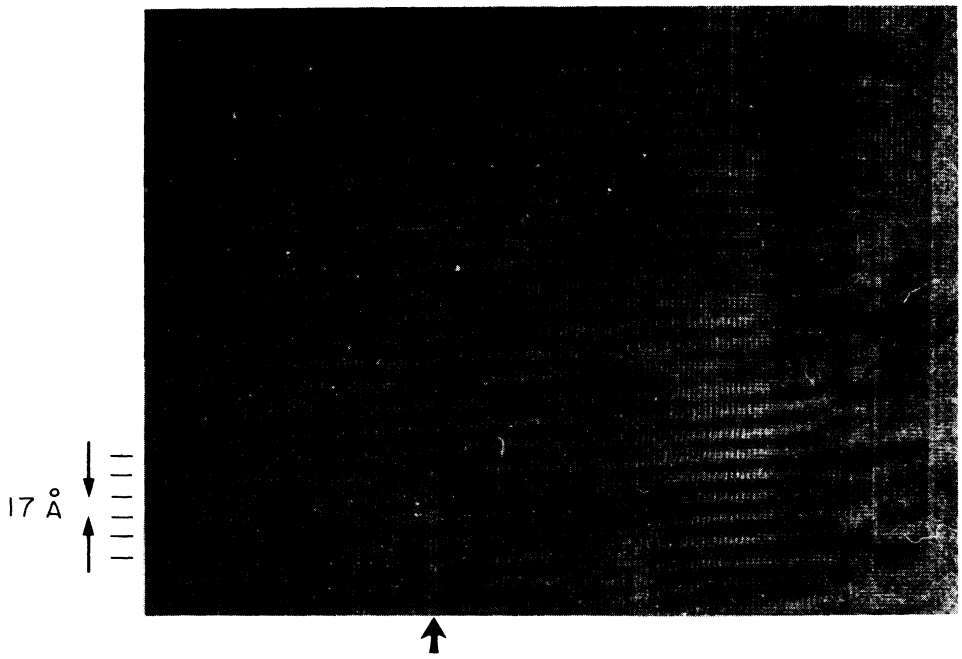

FIG. 4. Structure image corresponding to the diffraction image shown in Fig. 3, with c on the vertical axis. Small white spots correspond to the projected Fe sublattice. The edge of the crystal is on the right side of the picture. On its left side, Moiré fringes appear parallel to the Fe sublattice, with a period of $L^{\text{dens}} \simeq 17$ Å. The arrow indicates a dislocation.

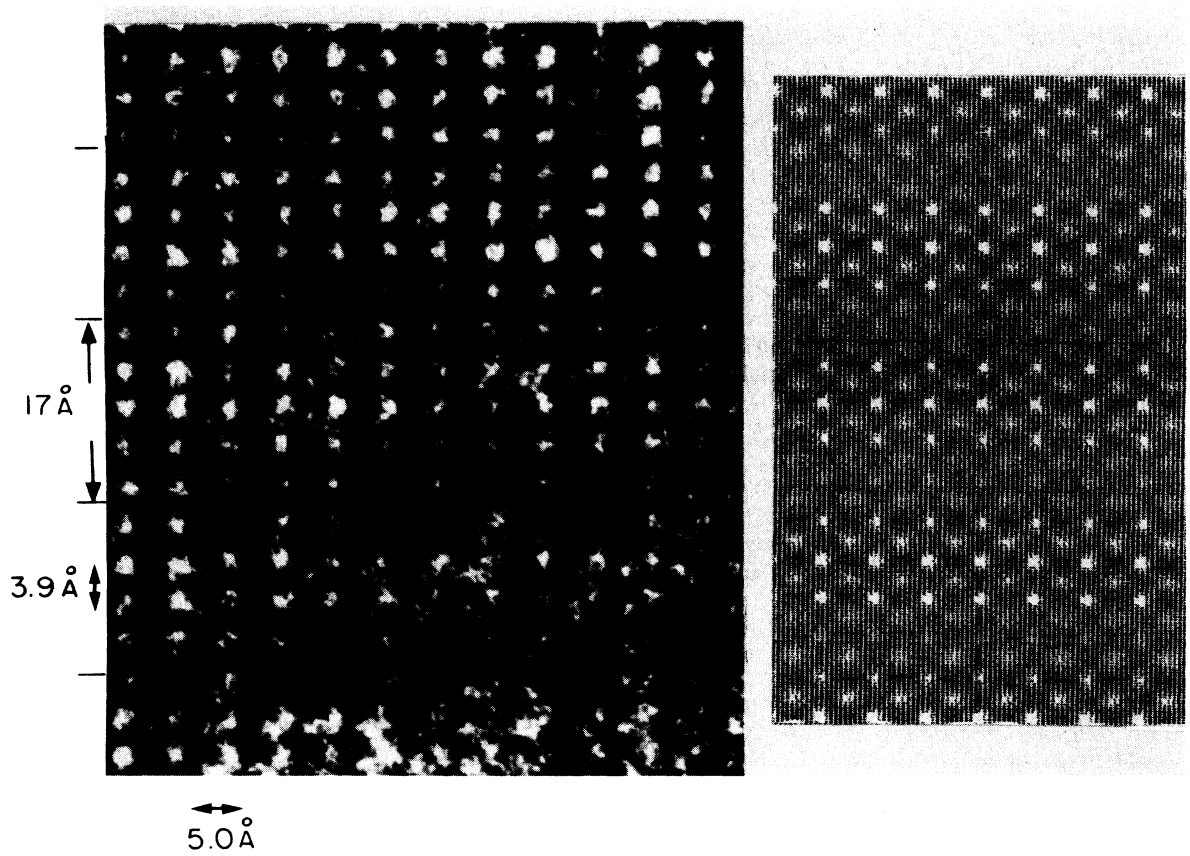

FIG. 5. Enlarged structure image and corresponding calculated image for a sample thickness of 50 Å and a defocus value of −580 Å. Same orientation as Fig. 4. White spots correspond to the projection of the Fe sublattice potential. They are 3.9 Å apart along [001] ($=c_{Fe}$) and 5.0 Å apart along [110] ($=a^{1/1}$).

structure, and of characteristic fringes perpendicular to c, which results from the superposition of the Fe and Nd substructures with different translation periods along that direction. Their spacings corresponds to the inverse effective reciprocal lattice vector $(2/c_{Nd}-2/c_{Fe})^{-1}\simeq 17$ Å. The fringes are distorted near the edge of the crystal, corresponding to rotational Moiré patterns. An enlarged portion of the undistorted part of the observed structure image and the corresponding simulated structure image are shown in Fig. 5. None of the observed images revealed any indication for regularly spaced stacking faults or commensurately spaced structure segments.

IV. DISCUSSION

The above results confirm that $Nd_{1+\epsilon}Fe_4B_4$ has tetragonal symmetry and belongs to the composition-modulated structure series of structure type $Sm_{1+\epsilon}Fe_4B_4$.[5,6] Its atomic arrangement is closely related to that of the Co-based tetragonal borides of structure type $NdCo_4B_4$.[23] Both structure types are characterized by parallel chains of edge-sharing transition-metal tetrahedra with attached B-atom pairs, and strings of rare-earth (R) atoms. In contrast to the Co series, the Fe series contains more than one rare-earth atom per transition-metal tetrahedron, so that the R-atom strings are more closely packed along the tetragonal axis, thus leading to nearly uncoupled, modulated, and incommensurate substructures.

A. Incommensurability and composition

Arguments in favor of incommensurate substructures in the Fe series are the ratios between the experimentally measured sublattice periods, $k=c_{Fe}/c_R$, which differ significantly between various crystals of the same compound and cannot be approximated by ratios of small integer values m/n. Further support comes from the absence of regularly spaced stacking faults or commensurately spaced structure segments in the electron-microscope structure images of $Nd_{1+\epsilon}Fe_4B_4$. The continuous structure deformations observed near the edges of the crystals are presumably due to a relaxation of the Nd-atom strings, and corroborates the presumed weak interactions of the Nd and Fe substructures. Furthermore, measurements of k as a function of temperature show no significant variation, as expected from a structure model which relates this parameter k to composition. The sublattice translation periods c_{Fe} and c_R of the three crystals measured for this work and those reported on other crystals in previous works[6,11,24,25] are plotted as a function of

the size of the R atom[26] in Fig. 6. The scattering of the data for the Nd and Gd crystals (dotted lines) and the quasi continuous variation for the other R (solid lines) can be interpreted in terms of small differences in rare-earth content (existence of a small homogeneity range), and of the influence of the R atomic size. For the Nd crystals, the sublattice translation ratios $k = c_{Fe}/c_{Nd}$ vary between the limits $1.109 \leq k \leq 1.143$, corresponding to an hypothetical difference of about 0.3 at. % in Nd content. Such a small homogeneity range is hard to verify by independent analytical methods. The assumption of incommensurate substructures (i.e., corresponding to irrational k values) made in this work, where composition is the critical parameter, leads to compounds of variable composition such as $Nd_{1+\epsilon}Fe_4B_4$ ($1.11 \leq k = 1+\epsilon \leq 1.14$). This contrasts sharply with the assumption of superstructures (i.e., corresponding to rational k values) made by other authors,[11] according to which k depends only on the type of rare-earth used, thus leading to compounds of well-defined composition such as $Nd_5Fe_{18}B_{18}$ and $Gd_2Fe_7B_7$.

B. Symmetry

In view of the above arguments, the two commensurate-structure models used so far to describe the structural series $R_{1+\epsilon}Fe_4B_4$ are only approximations. The tetragonal model used in this work for $Nd_{1+\epsilon}Fe_4B_4$ which is that used originally for $Sm_{1+\epsilon}Fe_4B_4$,[5,6] and the orthorhombic one used later for $Nd_5Fe_{18}B_{18}$ and $Gd_2Fe_7B_7$,[11] both have the same general formula $R_m(Fe_4B_4)_n$, but they differ with respect to lattice symmetry ($P4_2/n$ and $Pccn$, respectively) and allowed integer values for m and n (m and n odd for the tetragonal model, m even and n odd for the orthorhombic one). The tetragonal model appears to be the better choice for the following two reasons. Firstly, none of the experimental data presented so far shows evidence for a lowering of the structural symmetry from tetragonal to orthorhombic. Secondly, the tetragonal model is more flexible than the orthorhombic one with respect to the approximation of the various experimental sublattice parameter ratios k, because it allows a larger number of possible ratios m/n ($\simeq k$), within a given range of k.

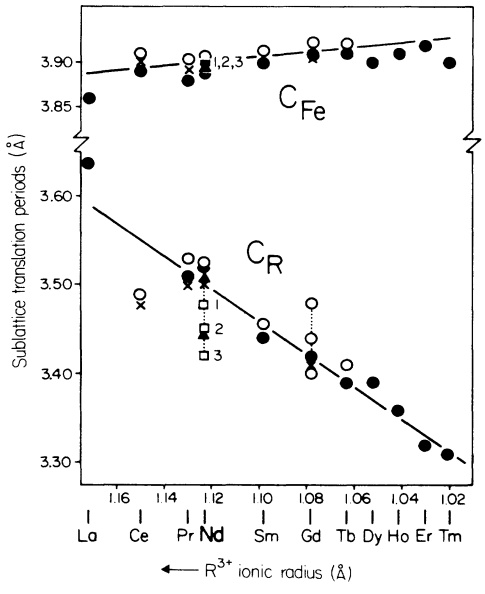

FIG. 6. Sublattice translation periods, c_R and c_{Fe}, as a function of atomic size of R^{3+} (Ref. 26). Data for Nd and Gd (dotted lines) refer to different samples. Open squares, this work; open circles, Ref. 6; crosses, Ref. 11; solid triangles, Ref. 24; solid circles, Ref. 25.

C. Modulations

The data presented in this work suggest that the periods of the various structure modulations observed both by x-ray (rotational and displacive) and electron diffraction (density) depend on the *sub*lattice translation periods $\mathbf{c}_R$ and $\mathbf{c}_{Fe}$ rather than on the *super*lattice translation period $c \simeq m\mathbf{c}_R \simeq n\mathbf{c}_{Fe}$ of the commensurate-structure model used for structure refinement. This is illustrated by the relation

$$L^{rot} = 2L^{dis} = 2L^{dens} = 1/(1/c_{Nd} - 1/c_{Fe}) ,$$

which presumably also holds for the other members of this structural series. A different conclusion was reached by the authors of the orthorhombic model who assume that $L^{rot} = mc_R = nc_{Fe} = c$, i.e., the rotational modulation period is identical to the superlattice period (e.g., $Nd_5Fe_{18}B_{18}$: $c = 10c_{Nd} = 9c_{Fe} = 35.07$ Å). These authors also conclude the nonexistence of any displacive modulation, in contrast to our results which show that neither the Fe-atom tetrahedra nor the R atoms are equally spaced along the chain axis.

As to the amplitudes of the various modulations, our results suggest that they depend mainly on the nature of the rare-earths. For example, the amplitude of the rotational modulation of the Fe tetrahedra chains in $Nd_{19}(Fe_4B_4)_{17}$ [$\pm 0.16(2)$ Å] is larger than that found for $Sm_{17}(Fe_4B_4)$ [$\pm 0.11(2)$ Å].[6] The amplitudes of the displacement modulations of the Fe and Nd substructures in our Nd crystal [$\pm 0.06(1)$ and $\pm 0.05(2)$ Å, respectively] are not as well defined as that of the rotational modulation, but the data (e.g., Fig. 1) leave no doubt about the existence of these displacive modulations. Note that the minima of the displacement modulation of the Fe double tetrahedra coincide with the extrema of their rotational modulation (Fig. 2).

D. Interatomic distances

As expected, the interatomic distances derived from the refined tetragonal model $Nd_{19}(Fe_4B_4)_{17}$ differ significantly from those derived from the nonrefined orthorhombic model $Nd_5Fe_{18}B_{18}$. For example, the shortest Nd-Nd, Nd-Fe, and Fe-Fe distances in each of the substructure segments of $Nd_{19}(Fe_4B_4)_{17}$ have ranges of 3.44–3.53 Å, 2.85–2.98 Å, and 2.35–2.63 Å, respectively, compared to nearly constant values of about 3.50, 2.93, and 2.48 Å, respectively, as reported for $Nd_5Fe_{18}B_{18}$.[11]

In $Nd_{19}(Fe_4B_4)_{17}$, the shortest Fe-Fe distances within the various Fe_4 tetrahedra usually occur along shared tetrahedra edges (2.35–2.63 Å). The second shortest Fe-

Fe distances are usually those along unshared edges (2.55–2.74 Å), whereas the third shortest ones usually occur between adjacent tetrahedra chains (2.66–2.88 Å). The shortest Nd-Fe distances (2.85–2.98 Å) are consistent with those found in other intermetallic compounds containing Nd and Fe, while the Nd-Nd distances (3.44–3.53 Å) are significantly shorter than those in elemental Nd (3.64 Å) and in $NdCo_4B_4$ (3.82 Å), thus suggesting that these atoms interact strongly along the tetragonal axis. The distances between the boron atoms (1.6–2.2 Å) are consistent with pair formation.[27] The metal-boron distances are approximately 2.7 Å (Nd) and 2.0 Å (Fe).

E. Origin of the structural modulations

The presence of structural modulations in the Fe series $R_{1+\epsilon}Fe_4B_4$, and their absence in the Co series RCo_4B_4 is puzzling. A factor which could account for this difference is the steric hindrance between the transition-metal tetrahedra and the R-atom strings which are more closely packed in the Fe series than those in the Co series. Such a factor would be consistent with the larger rotational amplitude found for the Nd compound, compared to that found for the Sm compound, which can be attributed to the larger metallic radius of Nd (1.821 Å) compared to that of Sm (1.804 Å).[28] Moreover, Nd-Fe distances in the modulated structure are 0.1 Å larger, on the average, than those calculated for a nonmodulated structure model. A question which remains to be answered is why the structures of the Fe series allow to accommodate more than one R atom per Fe_4 tetrahedron, and why those of the Co series do not. Phases with $NdCo_4B_4$-type structure have been found so far mainly for light rare-earth elements and group-IX transition elements such as Co (La, Pr, Nd, and Sm) (Ref. 23) and Ir (Y, La, Ce, Pr, Nd, Sm, Eu, Gd, and Tb),[29,30] and group-VIII transition elements such as Ru (La) (Ref. 31) and Os (La, Ce, Pr, Nd, Sm, and Eu).[29,30] For heavy rare-earth elements, phases with a closely related structure were found for Os (Y, Gd, Tb, Dy, Ho, Er, Tm, Yb, and Lu),[29] which were qualitatively described in terms of an eightfold superstructure of $NdCo_4B_4$ along the tetragonal axis, but are presumably identical to the $Sm_{1+\epsilon}Fe_4B_4$ type.[5,6] Phases with $Sm_{1+\epsilon}Fe_4B_4$-type structure have so far been reported only for group-VIII transition elements such as Fe (La, Ce, Pr, Nd, Sm, Gd, Tb, Dy, Ho, Er, and Tm).[5,6,25] In the course of this work, further members were discovered for Os [Gd, $k=1.133(3)$, and Y, $k=1.143(3)$], and also for group-VII transition elements such as Mn [Nd, $k=1.176(1)$]. The existence of representatives with Os, which has a much bigger atomic size than Fe, suggests that geometry may not be the only factor determining the stability and the structural modulations of this series. Electronic factors may also be important, such as that which governs the formation of phases with so-called "chimney-ladder" structure; see for example $Rh_{17}Ge_{22}$ (Ref. 32) and $MnSi_{2-x}$ (Ref. 33), which are composition-modulated electron compounds,[34] and have noncommensurate substructures. Very few other metallic composite crystals have been reported so far; see for example $Ba_p(Fe_2S_4)_q$,[35] and $Hg_{3-\delta}AsF_6$.[36]

ACKNOWLEDGMENTS

We thank L. Schellenberg for his help with the high-temperature diffraction experiments, R. Wessicken for skillfully taking electron diffraction and lattice images, M. Arita for making available his up-to-date multislice image calculation programs, and B. Künzler and F. Liniger for photographic work.

[1] M. Sagawa, S. Fugimura, H. Ymamoto, Y. Matsuura, and K. Hiraga, IEEE Trans. Magn. **20**, 1584 (1984).
[2] G. C. Hadjipanayis, K. R. Lauless, and R. C. Dickerson, J. Appl. Phys. **57**, 4097 (1985).
[3] K. Oesterreicher and H. Oesterreicher, J. Less-Common Met. **104**, L19 (1984).
[4] R. K. Mishra, J. K. Chen, and G. Thomas, J. Appl. Phys. **59**, 2244 (1986).
[5] H. F. Braun, M. Pelizzone, and K. Yvon, in *Proceedings of the VIIth International Conference on Solid Compounds of Transition Elements, Grenoble, 1982* (University of Grenoble, Grenoble, France, 1982), Vol. IIB, p. 11.
[6] A. Bezinge, H. F. Braun, J. Muller, and K. Yvon, Solid State Commun. **55**, 131 (1985).
[7] A. Janner and T. Janssen, Acta Crystallogr. Sect. A **36**, 408 (1980).
[8] N. F. Chaban, Y. B. Kuz'ma, N. S. Bilonizhko, O. O. Kachmar, and N. V. Petriv, Dopov. Akad. Nauk Ukr. RSR Ser. A **10**, 873 (1979).
[9] D. Givord, J. M. Moreau, and P. Tenaud, Solid State Commun. **55**, 303 (1985).
[10] D. Givord, J. M. Moreau, and P. Tenaud, J. Less-Common Met. **115**, L7 (1985).
[11] D. Givord, J. M. Moreau, and P. Tenaud, J. Less-Common Met. **123**, 109 (1986).
[12] Y. J. Chang and X. R. Quian , Phys. Status Solidi A **93**, 573 (1986).
[13] J. M. Stewart, P. A. Machin, C. W. Pickinson, H. L. Ammon, H. Heck, and H. Flack, Technical Report No. TR-446 (Computer Science Center, University of Maryland, College Park, Maryland, 1976).
[14] A. J. Skarnulis, E. Summerville, and LeRoy Eyring, J. Solid State Chem. **23**, 59 (1978).
[15] A. J. Skarnulis, J. Appl. Crystallogr. **12**, 636 (1979).
[16] M. Arita (unpublished).
[17] P. M. de Wolff, T. Janssen, and A. Janner, Acta Crystallogr. Sect. A **37**, 625 (1981).
[18] *International Table for Crystallography A,* edited by T. Hahn, (Reidel, Dordrecht, Holland, 1983).
[19] J. M. Cowley, *Diffraction Physics,* 2nd ed. (North-Holland, Amsterdam, 1981), p. 343.
[20] G. Thomas and M. J. Goringe, in *Transmission Electron Microscopy of Materials,* edited by G. Thomas and M. J. Goringe (Wiley, New York, 1979), p. 90.

[21]M. Korekawa, Habilitationsschrift, Naturwissenschaftliche Fakultät, Universität München, München, 1967.
[22]W. Horst, T. Tagai, M. Korekawa, and H. Jagodzinski, Z. Kristallogr. **157**, 233 (1981).
[23]Yu. B. Kuz'ma and N. S. Bilonishko, Dopov. Akad. Nauk Ukr. RSR, Ser. A **3**, 275 (1978).
[24]K. H. J. Buschow, D. B. Mooij, J. L. C. Daams, and H. M. Van Noort, J. Less-Common Met. **115**, 357 (1986).
[25]D. Niarchos, G. Zouganelis, A. Kostikas, and A. Simopoulos, Solid State Commun. **59**, 389 (1986).
[26]R. D. Shannon, Acta Crystallogr. Sect. A **32**, 751 (1976).
[27]T. Lundström, in *Boron and Refractory Borides,* edited by V. I. Matkovich (Springer-Verlag, Berlin, 1977), p. 358.
[28]W. H. Zachariasen, J. Inorg. Nucl. Chem. **35**, 3487 (1973).
[29]P. Rogl, Monatsh. Chem. **110**, 235 (1979).
[30]K. Hiebl, P. Rogl, and M. J. Sienko, Inorg. Chem. **21**, 1128 (1979).
[31]A. Grüttner and K. Yvon, Acta Crystallogr. Sect. B **35**, 451 (1979).
[32]W. Jeitschko and E. Parthé, Acta Crystallogr. **22**, 417 (1967).
[33]H. Q. Ye and S. Amelinckx, J. Solid State Chem. **61**, 8 (1986).
[34]W. B. Pearson, Acta Crystallogr. Sect. B **26**, 1044 (1970).
[35]J. T. Hoggins and H. Steinfink, Acta Crystallogr. Sect. B **33**, 673 (1977).
[36]A. J. Schultz *et al.*, Inorg. Chem. **17**, 646 (1978).

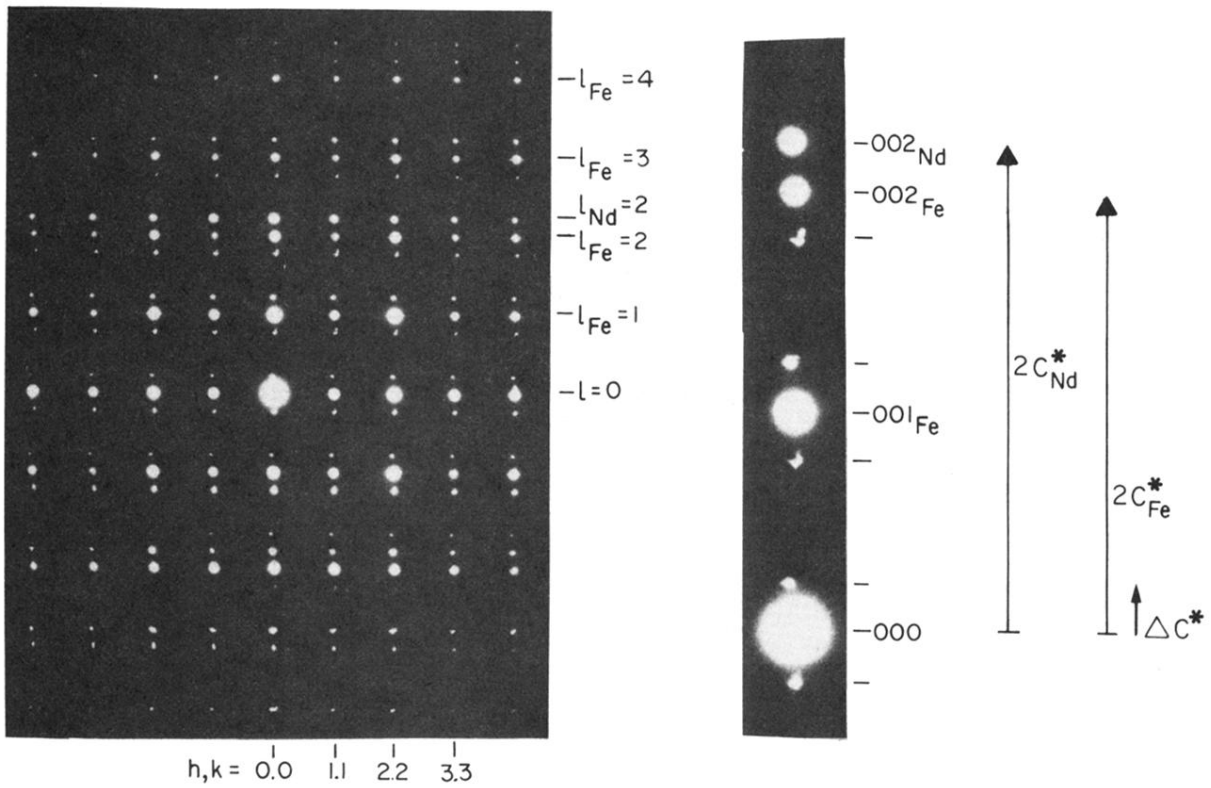

FIG. 3. (a) Electron-microscope diffraction image of $Nd_{1+\epsilon}Fe_4B_4$ along [110], with [001] as the vertical axis. (b) Enlarged portion of the diffraction image shown in (a).

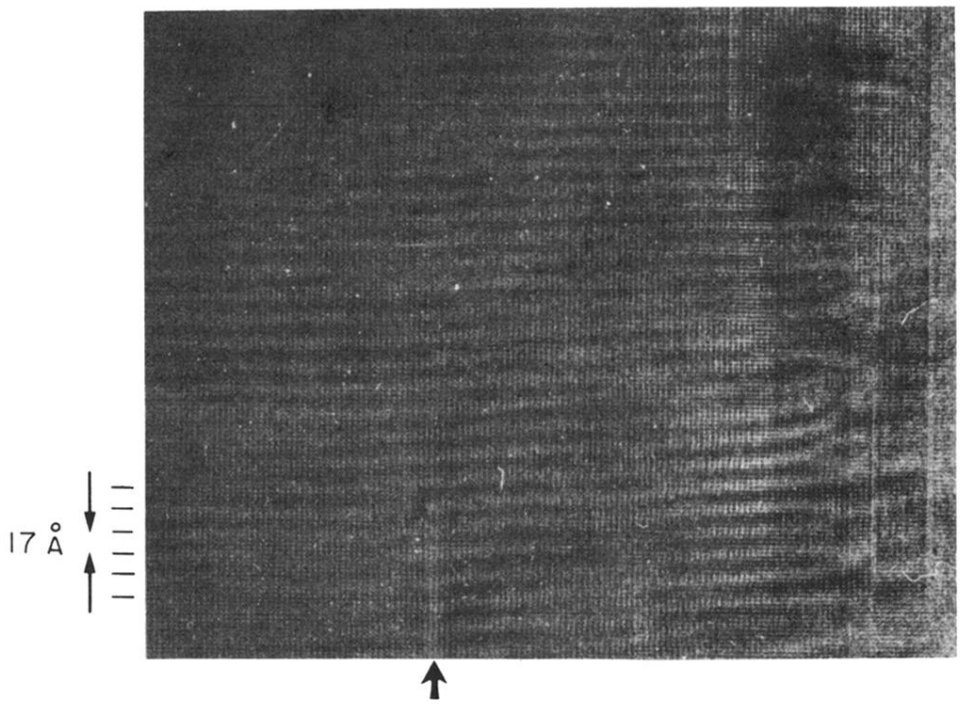

FIG. 4. Structure image corresponding to the diffraction image shown in Fig. 3, with c on the vertical axis. Small white spots correspond to the projected Fe sublattice. The edge of the crystal is on the right side of the picture. On its left side, Moiré fringes appear parallel to the Fe sublattice, with a period of $L^{\text{dens}} \simeq 17$ Å. The arrow indicates a dislocation.

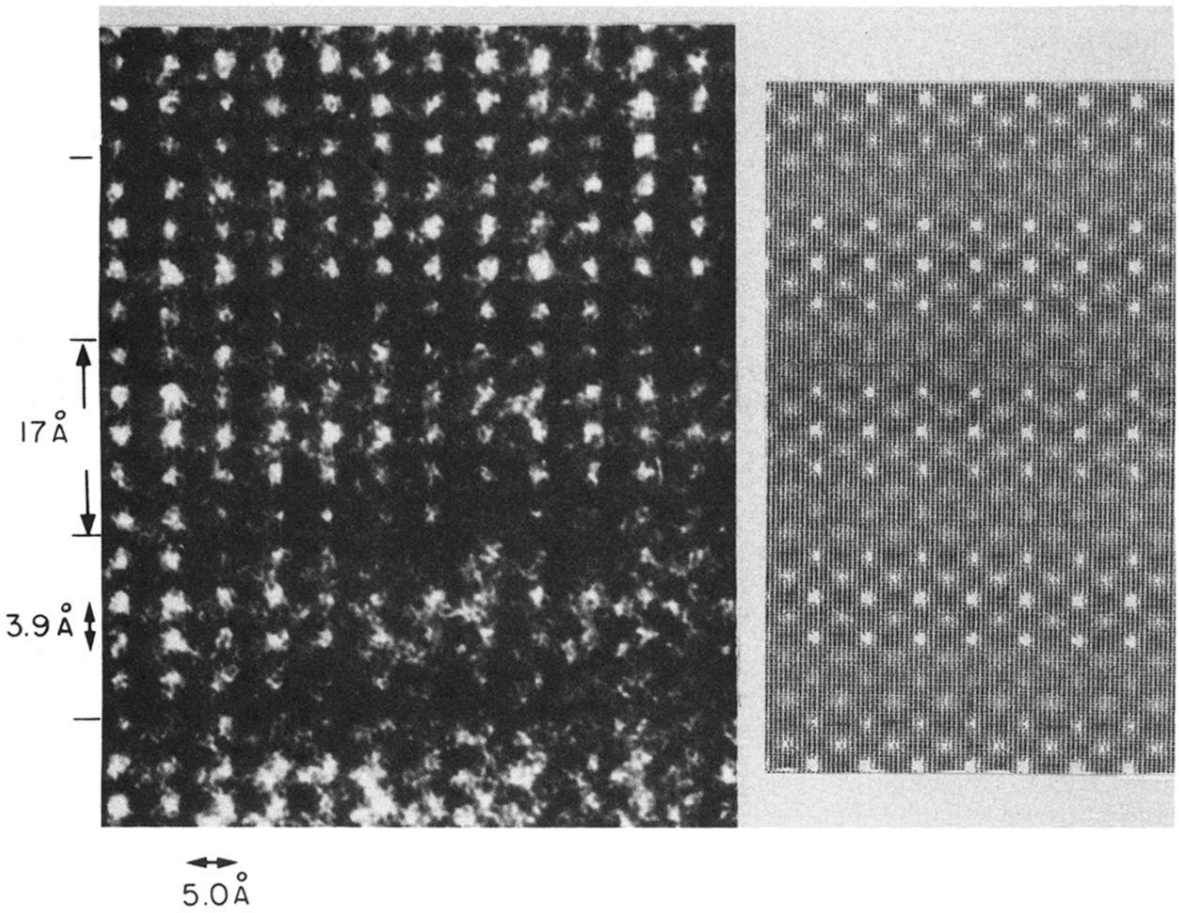

FIG. 5. Enlarged structure image and corresponding calculated image for a sample thickness of 50 Å and a defocus value of −580 Å. Same orientation as Fig. 4. White spots correspond to the projection of the Fe sublattice potential. They are 3.9 Å apart along [001] ($=c_{\mathrm{Fe}}$) and 5.0 Å apart along [110] ($=a^{1/1}$).